J. Appl. Comput. Mech., 9(4) (2023) 987-999
DOI: 10.22055/jacm.2023.42798.3978

ISSN: 2383-4536
jacm.scu.ac.ir

Shahid Chamran University of Ahvaz

Journal of Applied and Computational Mechanics

Research Paper

Theory and Experiment in Predicting the Strength of Hybrid Fiber Metal Laminates

Mustafa Babanli[1], Yunus Turen[2], Nurlan Gurbanov[1], Rafail Mehtiyev[3], Mustafa Yunus Askin[4], Mahmud Ismayilov[5]

[1] Department of Materials Science and Processing Technologies, Azerbaijan State Oil and Industry University, Azadlig 20, Baku, Az 1010, Azerbaijan
[2] Department of Metallurgical and Materials Engineering, Karabuk University, Turkey
[3] Department of General and Applied Mathematics, Azerbaijan State Oil and Industry University, Azadlig 20, Baku, Az 1010, Azerbaijan
[4] Materials Research and Development Center, Iron & Steel Institute, Karabuk University, Turkey
[5] Department of Mechanics, Azerbaijan State Oil and Industry University, Azadlig 20, Baku, Az 1010, Azerbaijan

Received January 16 2023; Revised March 27 2023; Accepted for publication March 28 2023.
Corresponding author: N. Gurbanov (nurlan.gurbanov@asoiu.edu.az)

Abstract. This article consists of three methodological stages. In the first one, a 3D numerical model of hybrid fiber metal laminates (FML) is developed inside ANSYS Workbench Explicit Dynamics modulus and used to predict their strengths according to the ASTM D3039M-17 standard. In the second stage, hybrid FMLs are produced according to the 4/3 stacking order in the laboratory environment, in line with the numerical model. Pure epoxy resin is initially used then reinforced with, 0.2% clay, GNP and SiO_2 nanoparticles: comparative tensile tests are carried out according to the above-mentioned standards. At the final stage, experimental data, computer and theoretical (analytical) models of nanocrack formation processes in 7075-T6 Al matrix nanoparticle-filled hybrid nanocomposite materials under the influence of high-speed and quasi-static deformation regimes are investigated. It is observed that there is a 5% difference between results from simulation and experiment.

Keywords: Hybrid composite, fiber metal laminates (FML), 7075-T6 Al, tensile test, ASTM D3039M-17, nanocrack, ANSYS Workbench.

1. Introduction

Composites can be defined as a combination of two or more materials that provide better properties compared to the base materials used separately. Unlike traditional materials, each material that makes up the composite preserves its unique physical, chemical and mechanical properties within the structure [1]. Since the mechanical performance of composite materials also depends on the internal structures of the materials and reinforcing particles [2], their behavior mostly depends on choosing the right combination of reinforcement materials [3-4]. Especially, the use of different nanoparticles as reinforcement elements in composites has revealed hybrid fiber metal laminated composites as a new generation of materials with the potential to meet the latest demands of advanced engineering applications [1, 5-6]. Hybrid FLM composite materials are formed by combining thin metal sheets and fiber-reinforced polymer materials [6].

Together with the developing technology, hybrid FML composites are designed with a practical manufacturing method based on the principle of superposition of layers created according to three-dimensional (3D) geometric data [7-9]. Finite element analysis, which is the most effective method compared to traditional test methods, is used to solve the balance, motion and deformation problems of physical solids in these kind of composite materials [10]. This method is based on the theories of continuum mechanics [8-11].

The ANSYS program ensures that the 3D model of the object exactly matches the material properties that will be used in reality [12]. The properties of materials used in engineering structures can be determined directly before simulation [13-16]. The force-displacement behaviors of two different composite materials were compared experimentally and mathematically in the ANSYS program by Arriaga et al. [17]. They observed that the numerical solution and the experimental solution gave close results.

In parallel with the developments in materials science, thermal and experimental scientific studies continue at full speed to improve the properties of FML composites and their behavior in service conditions. When the scientific resources on this subject are examined, there are not many researches on aluminum alloy reinforced laminated composites [18].

With the rapid developments in the field of nanomaterials, nanoparticle additions are made on matrix or carbon fiber surfaces to increase the interfacial adhesion strength of FML composites.

Published online: April 08 2023

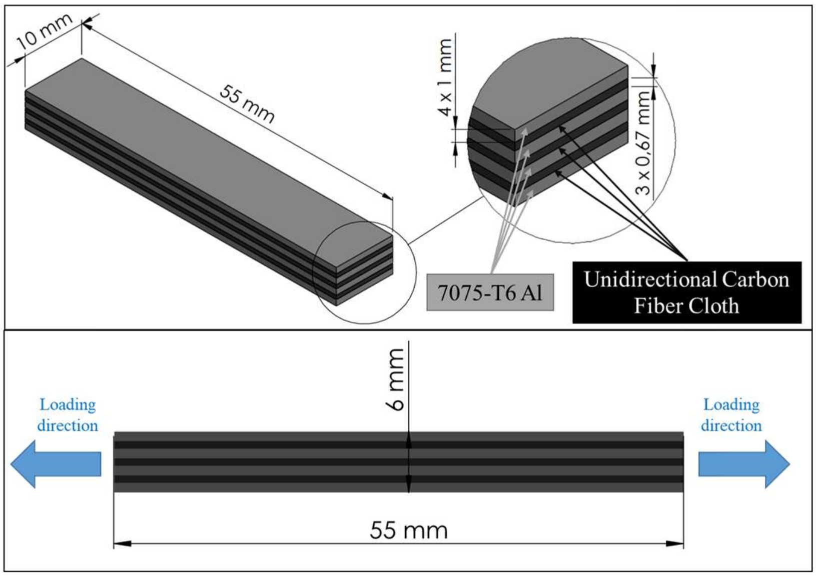

Fig. 1. Hybrid fiber metal laminated composite sample.

As a result of their investigations, Askin et al. [19] determined that the addition of 1% GNP to pure epoxy resin increased the tensile strength values of carbon fiber reinforced hybrid FML composites by approximately 9%. Gurbanov et al. [6] investigated the effect of 0.5% SiO_2 and clay addition to epoxy resin on the mechanical properties of carbon fiber reinforced hybrid FML composites. As a result of their investigations, they observed an increase of 6.49% and 1.17% in the tensile strength of hybrid FMLs.

The mechanical properties of nanocomposites are determined by the small size of the grains and high volume fraction occupied by the grain boundaries, which limits the movement of dislocations and initiates new plastic deformation and fracture mechanisms in the materials [20]. In particular, the high volume fraction of grain boundaries in nanocomposite materials is caused by the operation of deformation mechanisms, including grain boundary sliding [21, 22], diffusion creep across grain boundaries [23, 24] and grain boundary stress bonds. Therefore, the grain boundaries and their connections play a key role in the formation and development of cracks [25].

In this study, tensile tests of hybrid FML composites are carried out theoretically and experimentally according to ASTM D3039M-17, and the effects of nanoparticles used in composites on nanocracks formed under the influence of tensile test and quasistatic deformation regimes are investigated.

2. Material and Method

2.1 Materials (Theoretical and Experimental)

The 3D model for the composite prepared with the help of ANSYS program, unidirectional carbon fiber, epoxy resin and 1 mm thick 7075-T6 Al sheet were simulated according to the 4/3 stacking order in accordance with the material properties used in reality (Fig. 1).

2.1.1 Materials specifications

1. Matrix:

The matrix material in the composites is 7075-T6 Al sheet with a Young's Modulus of 70 GPa and a thickness of 1 mm. In addition to having high hardness and strength values, 7075-T6 Al sheet is an equivalent material to steel by maximizing these values due to its heat treatment feature.

2. Reinforcements:

a) Epoxy resin:

Epoxies consist of two or more epoxy-containing components. They are obtained by the reaction of polyphenol with epoxy chloride under basic conditions. They are in the form of a viscous and light-colored liquid. The transparent and sticky state is characteristic of amorphous polymers. It provides adhesion between the matrix and the fiber.

b) Carbon fiber:

Unidirectional carbon fiber fabric with a fiber density of 300 g/m^2 is widely used as a reinforcement element in hybrid fiber metal laminated composite materials.

In the experimental part of the article, as in the theoretical part, hybrid FML composite materials are 1 mm thick 7075-T6 Al sheet, reinforced with 2-layer carbon fiber fabric and 4/3 (Al / CF 0 ° - CF 0 ° / Al / CF 0 ° - CF 0 ° / Al / CF 0 ° - CF 0 ° /Al) is produced according to the stacking procedure. Hybrid FML composite materials were produced by mixing pure MGS-L326 epoxy resin and MGS-H265 hardener (100:25) at the first stage. In the subsequent production processes, 0.2% GNP (500 m^2/g, 99.5% pure), 15 nm thick (99%, 50% pure) SiO_2 nanoparticles and 18 nm thick nanoclay (%99,95 pure) are added to the epoxy resin. Hybrid FML composite materials were produced by pressing for 3 hours under a pressure of 1 ton at a temperature of 120°C in a protective gas environment.

2.2 Method (Theoretical and Experimental)

We created the mathematical model of the tensile test (Fig. 2) using the ANSYS Workbench Explicit Dynamics software package according to the ASTM D3039M-17 standard (Fig. 3). This software is based on finite element analysis (FEA). All materials for samples were chosen from software library.

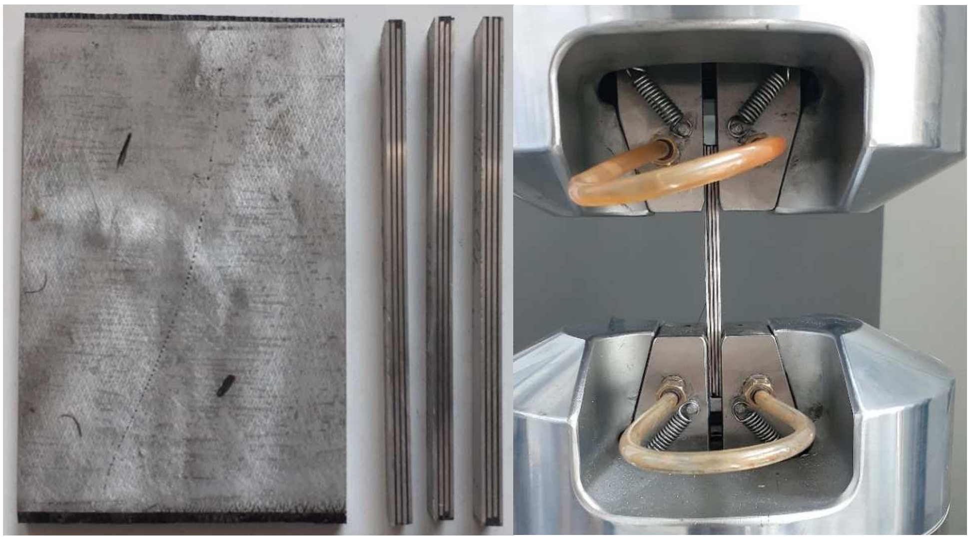

Fig. 2. Tensile test specimens.

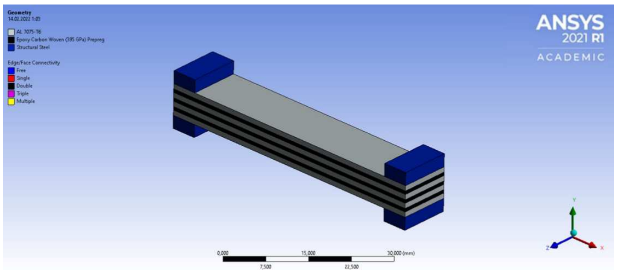

Fig. 3. 3D model of tensile test.

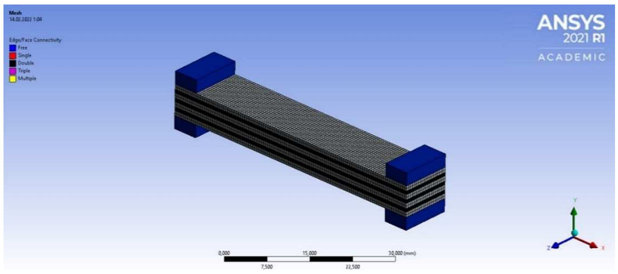

Fig. 4. Meshed tensile test sample.

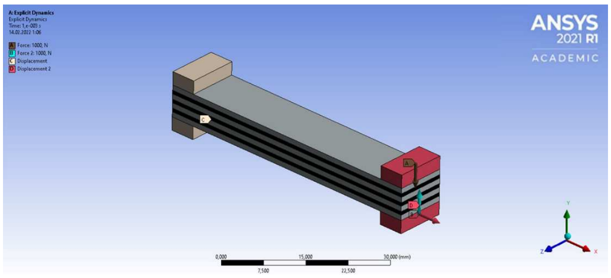

Fig. 5. Boundary conditions for tensile test sample.

Composite sample dimension was taken in accordance with ASTM D3039M-17 standard. Details of the required dimensions are given in Table 1 with the corresponding parameters.

Part 1

1) Composite samples:

Designed specimen is a nanocomposite material that consists of 4 layers of 7075-T6 Al sheet and 3 layers of unidirectional carbon fiber cloth. Material for 4 layers (1mm) of 7075-T6 Al sheet has been shown in Table 2 and material for 3 layers (0.67mm) of unidirectional carbon fiber cloth has been shown in Table 3.

2) Supports:

In tensile test for supports we used “Structural steel” material, with default parameters from ANSYS library which has been given in Table 4.

Part 2

3) Meshing:

For tensile test meshing was performed on the generated sample as shown in Fig. 4. In this tests we have meshing properties for specimens shown in Table 5. 49883 nodes and 3804 elements were used for full (specimen and supports together) model of tensile test meshing properties.

4) Boundary conditions:

Two support samples were fixed. On another two we applied the displacement equal to 25 mm and directed it in X axis direction. Forces are applied to the surface of the supports, compressing sample equal to 1000 N. These forces are directed against each other and parallel to the Y axis. Boundary conditions for tensile test has been shown in Fig. 5.

Table 1. Composite sample dimensions.

Parameter	Value
Length	55 mm
Width	10 mm
Thickness	6 mm

Table 2. Properties of 7075-T6 Al sheet.

Density kg/m³	Young's Modulus (GPa)	Poisson ratio	Shear Modulus (GPa)	Tensile Strength (GPa)
2804	70	0,32	26,7	0,48

Table 3. Properties of epoxy carbon woven (395 GPa) prepreg.

Density kg/m³	Young's Modulus (GPa)	Poisson ratio	Shear Modulus (GPa)	Tensile Strength (GPa)
1480	91,8	0,3	3	0,829

Table 4. Properties of structural steel.

Density kg/m³	Young's Modulus (GPa)	Poisson ratio	Shear Modulus (GPa)	Tensile Strength (GPa)	Bulk Modulus (GPa)
7850	200	0,3	70	0,2	166,7

Table 5. Specifications of different properties of specimen.

Properties	
Volume	3,3e-6 m³
Mass	0.00387 kg
Scale factor value	1
Bodies	7
Nodes	48951
Elements	30800
Mesh Metric	None

Table 6. Explicit Dynamics – Analysis Settings.

Type	Program Controlled
Step Controls	
Number Of Steps	1
Load Step Type	Explicit Time Integration
End Time	1e-003
Maximum Energy Error	0,1
Maximum Number of Cycles	1e+07

Table 7. Total Deformation results of specimen for tensile test.

Total Deformation (Tensile test)	
Results	
Minimum	0 mm
Maximum	0,62527 mm
Average	0,10507 mm
Minimum occurs on	Carbon fiber cloth
Maximum occurs on	7075-T6 Al

A mathematical model of hybrid FML composites was created using the ANSYS Workbench Explicit Dynamics software package and after the tensile tests were completed according to the ASTM D3039M-17 standard, the experimental part was passed. The tensile test at 1 mm/min, at 100 kN tensile of MTS brand according to a standard regarding the hybrid fiber was completed in production. It was carried out by removing 3 tensile samples of 1x10 cm size from one of the hybrid fiber metal plates. These items can be seen in Fig. 2.

3. Results and Discussion

ANSYS Workbench Explicit Dynamics module software was used to analyze the tensile test of the composite sample according to the ASTM D3039M-17 standard. The sample with the parameters, indicated in Tables 1-5 was used for tensile tests (Fig. 1). The process of meshing the specimen was carried out where the minimum size of the finite element was taken equal to 0.5 mm. The analysis settings are given in Table 6. The boundary conditions are shown in Fig. 5 and the results of simulation Figs. 6-7 are discussed in more detail in Part 1. The tensile tests result were indicated in Tables 7-9.

Part 1. Tensile test

Faizan et al. [26] The tensile behavior of four-layer composite materials with carbon fiber reinforced polymer matrix under 400 N tensile load was investigated using ANSYS software. For the total deformation, the composite specimen reinforced with epoxy resin and carbon fiber showed the least deformation, which was equal to 2.5311e-007 m. For maximum equivalent stress, the PVC Foam composite sample showed the lowest value equal to 41664 Pa. For the maximum normal stress, the PVC Foam composite sample showed the lowest value equal to 47476 Pa.

In this study, we investigate a tensile behavior of the composite material which consists of 4 layers of 7075-T6 Al sheet and 3 layers of unidirectional carbon fiber cloth. After simulation of tensile test, we got results which are shown in Figs. 6-7. Figure 8 shows a simulation of total deformation where the maximum value occurred on the "Al 7075-T6" and was equal to 0.62527 mm (Table 7). Figure 7 shows a simulation of equivalent stress where the maximum value occurred on the "Carbon fiber cloth" and was equal to 958,29 MPa (Table 8). Figure 8 shows a simulation of equivalent elastic strain where the maximum value occurred on the "Carbon fiber cloth" and was equal to 1,3481 mm/mm (Table 9).

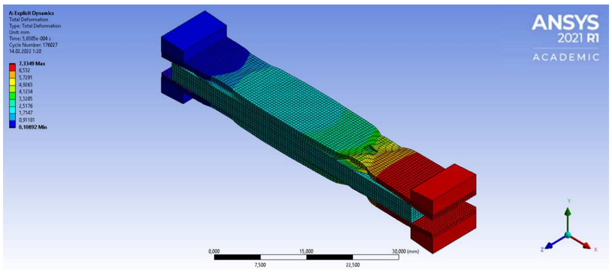

Fig. 6. Total deformation for tensile test sample.

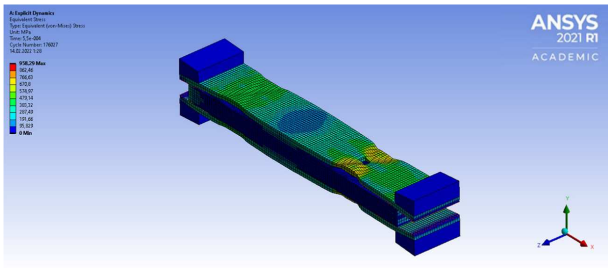

Fig. 7. Equivalent stress for tensile test sample.

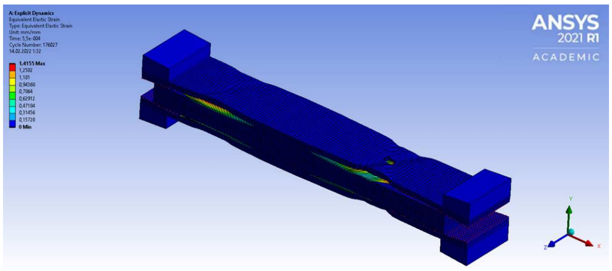

Fig. 8. Equivalent elastic strain for tensile test sample.

The tensile test results of hybrid FML composite materials according to ASTM D3039M-17 standard are given in Fig. 9. The tensile strength of hybrid FML composite produced with pure epoxy is 911.4 MPa. The tensile strength values of hybrid FML composites produced with 0.2% nanoclay added epoxy were 914.2 MPa. It was observed that 0.2% nanoclay particle reinforcement caused an increase of approximately 0.3% in the tensile strength values of the composites compared to hybrid FML composites produced with pure epoxy resin. Binu et al. [27] investigated the effects of nanoclay addition at different rates on the mechanical properties of composite materials and observed that 0.5% to 1% nanoclay addition positively increased the tensile modulus and tensile strength of composite samples. It was observed that the tensile strength of hybrid FML composites produced with 0.2% graphene added epoxy was appropriately 918.5 MPa, it was observed that the tensile strength of these hybrid FML composite materials increased by 0.8% compared to hybrid FMLs produced with pure epoxy. Sydlik et al. [28] in their study, observed that the addition of 1% carbon nanotube to the epoxy resin provides an improvement in the tensile strength of about 50%. As a result of the research, it has been observed that the addition of GNP to pure epoxy resin has a positive effect on the tensile properties of composite samples [1-14]. The experiments, showed that the tensile strength of hybrid FML composite materials produced with 0.2% SiO_2 added epoxy increased by 2.1%, which is appropriate compared to the hybrid FML composite material produced with pure epoxy. Afrouzyan et al. [29] observed the positive effects of different ratios of SiO_2 nanoparticle reinforcement on the tensile properties of glass epoxy resin composites. It was observed that as the ratio of SiO_2 nanoparticles added to glass/epoxy composites increased, there was a decrease in the tensile strength values of the composites. It was observed that 0.5% SiO_2 nanoparticle reinforcement provided the best effect on the tensile properties of composite materials.

If a homogeneous distribution of nanoparticles is provided in the epoxy resin, which is used as a matrix material in composites, it can contribute positively to the adhesion properties of the composite by preventing the progression of the crack that starts to form in the matrix [13]. Therefore, the positive change in the tensile strength of the material with the nanoparticle reinforcements obtained in this study can be attributed to this situation.

Consider a nanocrystalline solid consisting of nanoparticles with a long blunt crack and grain boundaries separating them (see Fig. 10.a). Suppose that a nanocrystalline solid is subjected to a uniform tensile load. The cross-section of a typical fragment of a nanocrystalline solid is shown in Fig. 10.a, and the crack intersects the grain boundary at a distance from the nearest junction (Fig. 11) [30].

Table 8. Equivalent Stress results of specimen for tensile test.

Equivalent Stress (Tensile test)	
Results	
Minimum	0 MPa
Maximum	958,29 MPa
Average	167,71 MPa
Minimum occurs on	Carbon fiber cloth
Maximum occurs on	Carbon fiber cloth

Table 9. Equivalent Elastic Strain results of specimen for tensile test.

Equivalent Elastic Strain (Tensile test)	
Results	
Minimum	2,6674e-005 mm/mm
Maximum	1,3481 mm/mm
Average	4,5171e-002 mm/mm
Minimum occurs on	7075-T6 Al
Maximum occurs on	Carbon fiber cloth

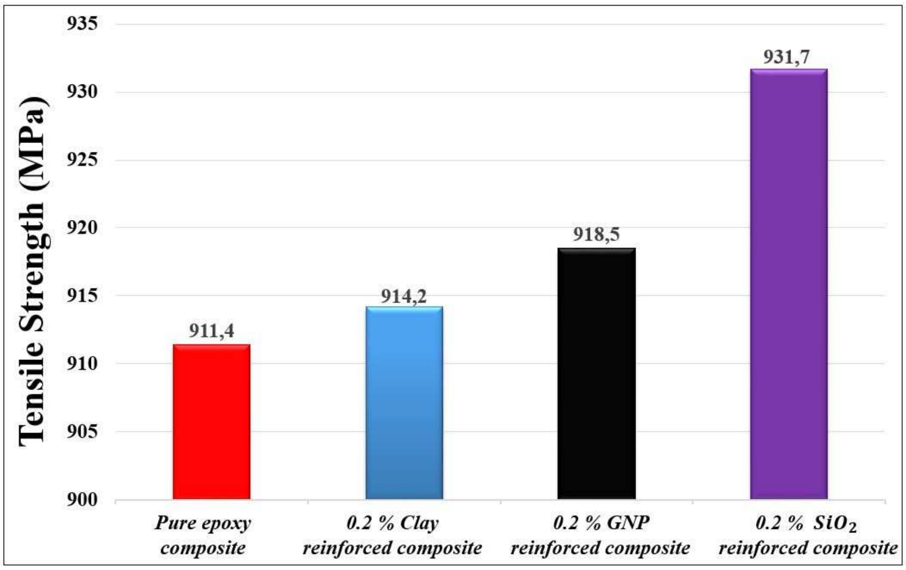

Fig. 9. Tensile test results of hybrid FML composites.

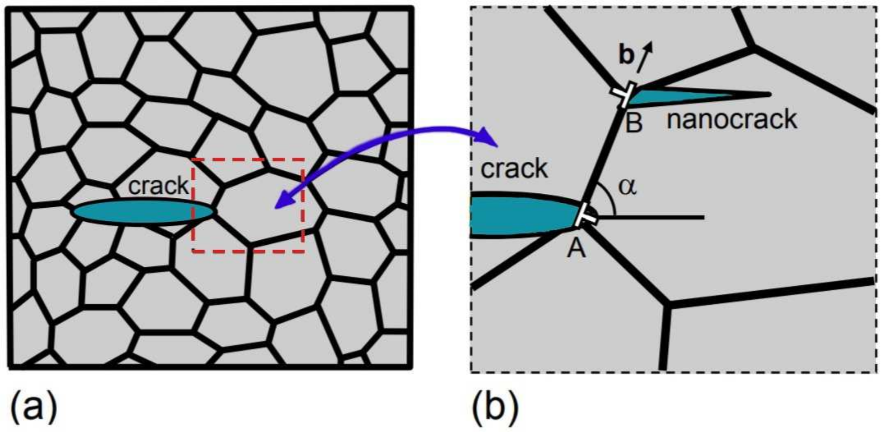

Fig. 10. Elliptical crack in deformable hybrid FML nanocrystalline materials. (a) overview, (b) sliding of the grain boundary along the AB boundary near the top of the long crack [30].

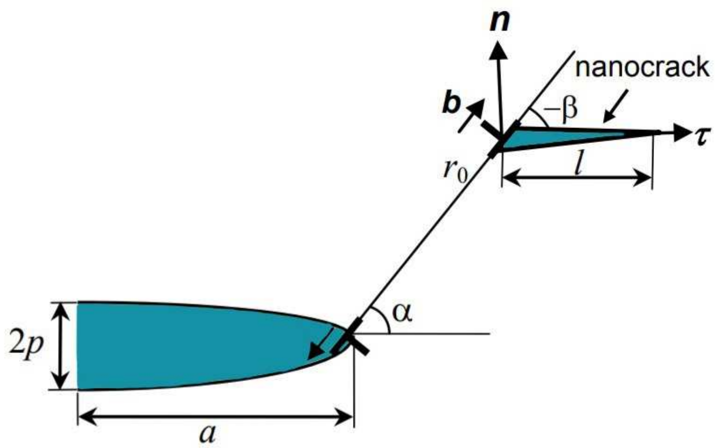

Fig. 11. Geometric view of a nanocrack formed as a result of dislocation near the apex of a long elliptical crack [26].

The stresses acting on the crack peak in the deformed body cause the grain boundaries to slip along *AB* (Fig. 10.b) and other grain boundaries near the end of the crack. In this case, the combination of β prevents the grain boundary from sliding along the *AB* grain boundary, resulting in the grain boundary slip causing incomplete plastic displacement near this joint. From the point of view of the theory of defects of solids, this combination preserves the dislocation, and the size of the Burgers vector increases in the process of sliding the boundary of the grain [30].

If the value of the Burgers vector *b* of the dislocation is large enough, nanocracks appear in the voltage field of the dislocation (Fig. 10.b). Studies [25] have shown that in uneven blunt cracks, the stresses near the crack peak are large enough to form a nanocrack and small enough to cause dislocations with the Burgers vector. This is due to the fact that the growth of the blunt crack occurs at a relatively low voltage level, which is not sufficient for the formation of dislocations with the Burgers vector. At the same time, the situation may change if the crack is blunt as a result of cage dislocations from the top of the crack or the previous emission of the grain border sliding on this peak. The stress required for the crack to grow is relatively high. For this reason, the local (local) stresses near the peak of the blunt crack may be significantly higher than the stresses near the blunt crack of the same length. Therefore, in the future, we will analyze the formation of nanocracks on the dislocation caused by the formation of the grain boundary as a result of landslides at the junction of the grain boundaries near the apex of the condensed crack (Fig. 11) [30].

In Fig. 8, we will model a blunt roof in the form of an elongated ellipse with a radius of curvature ρ of the vertex of the crack, which is smaller than the major semicircle a of the ellipse formed in hybrid FML nanocomposites.

The radius of curvature of the ρ crack is related to a and p, the half-axes of the ellipse, with $\rho = p^2 / a$ [30, 31-32]. We will model the fragmented nanocrystalline material with a modulus G and Poisson ratio ν as an elastic isotropic medium.

Let us now consider the grain boundary sliding near the apex of the condensed crack, causing dislocation with the Burgers b vector in hybrid FML nanocomposite compounds. Assume that the grain boundary where the landslide occurs is at an angle α to the crack plane (Fig. 11). In this case, the elliptical crack has a finite length, and the grain boundary sliding along the boundary of grain *AB* creates two dislocations that form a dislocation dipole (Fig. 10.b).

This dipole consists of the Burgers b vector dislocation formed by dislocation with the Burgers b vector located in the hybrid FML nanocomposite compound and the inside of the crack (Fig. 11). In fact, the formation of the second dislocation has an elliptical rift. At equilibrium, the value of the burgers vector b of the dislocation dipole corresponds to the minimum energy ΔW associated with the formation of the dipole. In other words, the equilibrium value of the burgers vector b_c is determined by the relation $\partial(\Delta W) / \partial b |_{b=b_c} = 0$ [29].

In this case, the energy ΔW is determined by the following equation:

$$\Delta W = W_S + W_C - A \tag{1}$$

where W_S is the specific elastic energy of the dislocation dipole, W_C is the energy of dislocation with the Burgers *b* vector, and A is the work of the displacement voltage generated by the external load based on the formation of the dislocation dipole.

The specific elastic energy of the dislocation dipole is given [32]:

$$W_s = -\frac{b}{2}\int_0^{r_0 - r_c} \sigma_{r\theta}^{dip}(r, \theta = \alpha) dr, \tag{2}$$

where $r_c \approx b$ is the radius of the dislocation nucleus and $\sigma_{r\theta}^{dip}$ the peak of the crack, which is the beginning of the stress tensor (0, 0) in the cylindrical coordinate system (r, θ) formed by the dislocation, creates a dislocation dipole of a solid with an elliptical crack (Fig. 12).

The second limit W_C, $W_C \approx Db^2 / 2$ is determined by the relation, where $D = G / [2\pi(1-\nu)]$ [33]. The final limit in Eq. (1) is calculated by the following equation [34]:

$$A = b\int_0^{r_0} \sigma_{r\theta}^{e}(r, \theta = \alpha) dr, \tag{3}$$

where $\sigma_{r\theta}^{e}$ are the components of the tensile tensor that generates the external mechanical load σ_0 near the peak of the elliptical crack.

The equilibrium value of the modulus *b* of the burgers vector is calculated by equations (1) to (3) using the condition $\partial(\Delta W) / \partial b |_{b=b_c} = 0$. As a result, we get the following expression [34]:

$$b_c = \left(\frac{\sigma_0}{D}\right) f(r_0, \rho, \alpha),$$

where

$$f(r_0, \rho, \alpha) = \frac{\int_0^{r_0} \bar{\sigma}_{r\theta}^{e}(r, \theta = \alpha) dr}{1 - \int_0^{r_0 - r_c} \bar{\sigma}_{r\theta}^{dip}(r, \theta = \alpha) dr}. \tag{4}$$

Now let's calculate the external voltage σ_0 required to form the dislocation dipole (Fig. 8) with the modulus b_c of the Burgers vector. If the total tensile stress σ_p, i.e. $\sigma_{yy} = \sigma_p$ around the crack peak, reaches a critical value, the elliptical crack growth can be assumed [35]. The equation $\sigma_{yy} = \sigma_p$ is true when the external voltage σ_0 reaches a maximum value of σ_{0c}. Thus, the equation under study is true when the radius of the peak of the crack ρ, ρ_c sometimes exceeds the critical size.

If the critical radius is given in the form $\rho_c = 16G\gamma / [\pi(1-\nu)\sigma_p^2]$ (γ – specific energy of the free surface) [36], this value for the *Al* material will be approximately 1.4 nm.

At the apex of the crack, the voltage σ_{yy} is the sum of the voltage σ_{yy}^{e} determined by the external load and the voltage σ_{yy}^{dip} generated by the dislocation dipole, mathematically, $\sigma_{yy} = \sigma_{yy}^{e} + \sigma_{yy}^{dip}$. The following expression for the voltage σ_{yy}^{e} is known [35]:

$$\sigma_{yy}^{e}(x = a, y = 0) = 2\sigma_0\sqrt{\frac{a}{\rho}}. \tag{5}$$

Substituting the equation (5) and the relation $\sigma_{yy} = \sigma_{yy}^{e} + \sigma_{yy}^{dip}$ in the formula $\sigma_{yy} = \sigma_p |_{\sigma_0 = \sigma_{0c}}$ gives the following expression for the maximum value of the external voltage σ_{0c} [35]:

$$\sigma_{0c} = \frac{\sigma_p - Dbg(r_0,\alpha,\rho)}{2}\sqrt{\frac{\rho}{a}}, \tag{6}$$

where the function $g(r_0,\alpha,\rho)$ is given by the relation $\sigma_{yy}^{dip} = Db\bar{\sigma}_{yy}^{dip} = Dbg(r_0,\rho,\alpha)$.

In the case of $b = b_c$ and $\sigma_0 = \sigma_{0c}$, after substituting the expression $b_c = (\sigma_c / D) f(r_c,\rho,\alpha)$ in Eq. (6) and solving the final equation for σ_{0c}, we obtain the following expression [36]:

$$\sigma_{0c} = \frac{\sigma_p}{2\sqrt{\dfrac{a}{\rho}} + f(r_0,\alpha,\rho)g(r_0,\alpha,\rho)}, \tag{7a}$$

$$b_c = \frac{\sigma_p}{D}\frac{f(r_c,\alpha,\rho)}{2\sqrt{\dfrac{a}{\rho}} + f(r_0,\alpha,\rho)g(r_0,\alpha,\rho)}, \tag{7b}$$

The functions $f(r_0,\rho,\alpha)$ and $g_0(r_0,\rho,\alpha)$ depend on the stresses $\sigma_{r\theta}^{e}$, $\sigma_{r\theta}^{dip}$ and σ_{yy}^{dip} created by the external load σ_0 and the dislocation dipole in an infinitely elastic medium with an elliptical crack. From the scientific work [37], we find the following expressions for these tensions. The voltage $\sigma_{r\theta}^{e}$ generated by the elliptical crack in an infinitely elastic medium σ_0 is given mathematically as follows [38]:

$$\sigma_{r\theta}^{e} = \mathrm{Im}\left[\left(\bar{z}\,\phi_e''(z) + \psi_e'(z)\right)e^{2i\theta}\right],\ z = x + iy = a + re^{i\theta},\ i = \sqrt{-1}. \tag{8}$$

The functions $\phi_e(z)$ and $\psi_e(z)$ in Eq. (8) are complex variable potentials defined by the following equations [39]:

$$\phi_e = \frac{\sigma_0 R}{4}\left(\xi - (2+m)\frac{1}{\xi}\right), \tag{9a}$$

$$\psi_e = \frac{\sigma_0 R}{2}\left(\xi - \frac{1}{\xi} - \frac{(1+m)(1+m\xi^2)}{\xi(\xi^2 - m)}\right), \tag{9b}$$

where, $R = \sqrt{a}(\sqrt{a} + \sqrt{\rho})/2$, $m = (\sqrt{a} - \sqrt{\rho})/(\sqrt{a} + \sqrt{\rho})$, and ξ is one of the two roots of the equation $z = R(\xi + m/\xi)$, within the condition $|\xi| \geq 1$.

The stress field $\sigma_{ij}^{dip}(r,\theta)$ generated by the dislocation dipole in an infinitely elastic medium with an elliptical crack (Figs. 10 and 11) is calculated from the ratio $\sigma_{ij}^{dip}(r,\theta) = \sigma_{ij}^{d}(r_0,\alpha,r,\theta) - \sigma_{ij}^{d}(0,\alpha,r,\theta)$, where $\sigma_{ij}^{d}(r_0,\alpha,r,\theta)$ is the stress field resulting from the dislocation at point *B* (Fig. 10.b) and $\sigma_{ij}^{d}(0,\alpha,r,\theta)$ is the stress field resulting from the dislocation located inside the elliptical crack (Fig. 10.b).

The voltage $\sigma_{r\theta}^{d}(r_0,\alpha,r,\theta)$ is calculated from the following relation [36, 37]:

$$\sigma_{r\theta}^{d}(r_0,\alpha,r,\theta) = \mathrm{Im}\left[\left(\bar{z}\phi_d''(z) + \psi_d'(z)\right)e^{2i\theta}\right], \tag{10}$$

where

$$\phi_d(z) = A\ln(z - z_d) + \phi_{im}(z), \tag{11a}$$

$$\psi_d(z) = \bar{A}\ln(z - z_d) - A\frac{\bar{z}_d}{(z - z_d)} + \psi_{im}(z), \tag{11b}$$

$$\phi_{im}(z) = 2A\ln\xi - A\ln\left(\xi - \frac{m}{\xi_d}\right) - A\ln\left(\xi - \frac{1}{\xi_d}\right) + \bar{A}\frac{\xi_d\left(1 + m\bar{\xi}_d^2\right) - \bar{\xi}_d\left(\xi_d^2 + m\right)}{\xi_d\,\bar{\xi}_d\left(\bar{\xi}_d^2 - m\right)\left(\xi - \left(1/\bar{\xi}_d\right)\right)} \tag{12}$$

$$\phi_{im}(z) = 2\bar{A}\ln\xi - \bar{A}\ln\left(\xi - \frac{m}{\xi_d}\right) - \bar{A}\ln\left(\xi - \frac{1}{\xi_d}\right) + A\frac{\xi_d\left(\bar{\xi}_d^2 + m^3\right) - m\xi_d\left(\bar{\xi}_d^2 + m\right)}{\xi_d\,\bar{\xi}_d\left(\bar{\xi}_d^2 - m\right)\left(\xi - (1/\xi_d)\right)} - \xi\frac{1 + m\xi^2}{\xi^2 - m}\frac{d\phi_{im}}{d\xi}, \tag{13}$$

where $|\xi_d| \geq 1$, $z = a + re^{i\theta}$, $z_d = a + r_0e^{i\theta}$, $A = Gbe^{i\theta}/(4i\pi[1-\nu])$ is one of the roots of the equation $z_d = R(\xi_d + m/\xi_d)$, within the condition.

Similar to equation (10), we will write below the expressions for the stress tensor component σ_{yy}^{d}, σ_{nn}^{d} and $\sigma_{\tau n}^{d}$ [36, 37]:

$$\sigma_{yy}^{d}(r_0,\alpha,r,\theta) = \mathrm{Im}\left[2\phi_d'(z) + \bar{z}\phi_d''(z) + \psi_d'(z)\right], \tag{14}$$

$$\sigma_{nn}^{d}(r_0,\alpha,r,\theta) = \mathrm{Im}\left[2\phi_d'(z) + \bar{z}\phi_d''(z) + \psi_d'(z)e^{2i(\alpha+\beta)}\right], \tag{15}$$

$$\sigma_{\tau n}^{d}(r_0,\alpha,r,\theta) = \mathrm{Im}\left[\left(\bar{z}\phi_d''(z) + \psi_d'(z)\right)e^{2i(\alpha+\beta)}\right]. \tag{16}$$

It is given by equations (15) and (16) where the indices "d" at voltages σ_{nn}^{e} and $\sigma_{\tau n}^{e}$ are replaced by indices "e".

As a result, the expressions for the stresses $\sigma_{r\theta}^{dip}$, σ_{yy}^{dip}, σ_{nn}^{dip} and $\sigma_{\tau n}^{dip}$ are obtained from the equations (10) to (16) and the relation $\sigma_{ij}^{dip}(r,\theta)=\sigma_{ij}^{d}(r_0,\alpha,\theta,r)-\sigma_{ij}^{d}(0,\alpha,\theta,r)$. The functions $f(r_0,\alpha,\rho)$ and $g_0(r_0,\alpha,\rho)$ are calculated from the above expressions, the equation (4) and the expression $g(r_0,\alpha,\rho)=\sigma_{yy}^{dip}/Db$.

Let us now consider the conditions for the formation and growth of a nanocrack on a dislocation in a hybrid FML nanocomposite compound near the apex of an elliptical crack (Figs. 10 and 11). Let us assume that the length of the nanocrack is l and the angle β is in the plane of the grain boundary where the grain boundary slip occurs. In the first approximation, we will consider the growth of nanocracks in the stress field created by the dislocation dipole between the nanocrack and the elliptical crack, and the load applied to the composite by the elliptical cracks. When we consider the growth of nanocracks, we will model it as a diffuse crack in an infinite body affected by a stress field. Thus, we will ignore the effect of the additional stress field created by the formation and growth of a large elliptical nanocracks.

We will use the next growth criterion of nanocrack to calculate the growth conditions of nanocracks [39]:

$$F>2\gamma_e, \tag{17}$$

where F is the configuration force, if the nanocrack grows within the grain, then $\gamma_e=\gamma$ if the nanocrack grows along the grain boundary, then $\gamma_e=\gamma-\gamma_b/2$ where γ_b is the specific energy of the grain boundary. The configuration force in the approximation used is calculated by the following equation [39]:

$$F=\frac{\pi l(1-\nu)}{4G}\left(\bar{\sigma}_{nn}^{2}+\bar{\sigma}_{\tau n}^{2}\right), \tag{18}$$

where τ is the vector directed to the dislocation line along the nanocrack, n the normally directed vector to the nanocrack (Fig. 11), σ_{nn} and $\sigma_{\tau n}$ the components of the dislocation dipole of the solid with elliptical crack and the field of stresses created by external load, $\bar{\sigma}_{nn}$ and $\bar{\sigma}_{\tau n}$ the average weight values of these stresses. The quantities $\bar{\sigma}_{nn}$ and $\bar{\sigma}_{\tau n}$ are determined by the following relations [39]:

$$\bar{\sigma}_{kn}=\frac{2}{\pi l}\int_0^l \sigma_{kn}\sqrt{\frac{\tau}{l-\tau}}d\tau, \quad k=n,\tau. \tag{19}$$

In addition to fulfilling the equation (18) for the growth of the nanocrack, we will require that the stress in the formation of the nanocrack is positive in the plane of the nanocrack. Considering Eq. (19) in Eq. (18), we rewrite the growth of the nanocrack under the condition $q>q_c$ and here, we get the expressions $q=(\pi l/2)(\bar{\sigma}_{nn}^{2}+\bar{\sigma}_{\tau n}^{2})$ and $q_c=4\gamma_e G/(1-\nu)$. The growth of nanoparticles in 7075-T6 aluminum matrix clay, SiO_2 and GNP filler hybrid FML nanocomposites was calculated using equations (18) and (19) based on the following parameters:

Parameters for 0.2% Glay:

$$\sigma_p=28.8\text{ MPa},\ \gamma=1.18\text{ Dj/m}^2,\ \nu=0.272,\ G=42\text{ MPa},\ a=2.5\ \mu\text{m},\ \alpha=\pi/3,\ \beta=\pi/2,\pi/4,0,\pi.\ \rho=1.0,\ 1.2,\ 1.4,\ 1.6. \tag{20}$$

Parameters for 0.2% GNP:

$$\sigma_p=28.8\text{ MPa},\ \gamma=1.07\text{ Dj/m}^2,\ \nu=0.182,\ G=32\text{ MPa},\ a=2.0\ \mu\text{m},\ \alpha=\pi/3,\ l=1.0,1.5,2.0,2.5,\ \beta=\pi/2,\pi/4,0,\pi.\ \rho=1.0,\ 1.2,\ 1.4,\ 1.6. \tag{21}$$

Parameters for 0.2% SiO_2:

$$\sigma_p=28.8\text{ MPa},\ \gamma=1.41\text{Dj/m}^2,\ \nu=0.132,\ G=58\text{ MPa},\ a=1\ \mu\text{m},\ \alpha=\pi/3,\ \beta=\pi/2,\pi/4,0,\pi.\ \rho=1.0,\ 1.2,\ 1.4,\ 1.6. \tag{22}$$

Figure 12 shows the dependences of $q(l)$ on different angle values $\beta=\pi/4,\pi/2,\pi$ corresponding to $r_0=1.0\text{nm}$, $r_0=1.2\text{nm}$, $r_0=1.4\text{nm}$, $r_0=1.6\text{nm}$ values for hybrid FML composites with 0.2% clay addition. The horizontal lines in the given graphs indicate the values of q_c. Nanocrack growth is energetically favorable in regions where $q(l)$ lies above the horizontal $q = q_c$ line. As can be seen from the graphs depicted in Fig. 12, the conditions for the origin and growth of nanocracks in nanocomposite materials ρ are proportional to the increase in the radius of curvature of the crack tip.

Along with the radius of curvature ρ of the crack tip, an important parameter affecting the origin and growth of the nanocrack is the distance from the blunt crack tip to the dislocation at the grain boundary junction. Fig. 13 shows $q(l)$ dependences for different values of $r_0=1.0\text{nm}$, $r_0=1.2\text{nm}$, $r_0=1.4\text{nm}$, $r_0=1.6\text{nm}$ corresponding to values of $\beta=\pi/4,\pi/2,\pi$ for hybrid FML composites with 0.2% SiO_2 addition. As it can be seen from Fig. 13, a sufficiently large increase of r_0 makes it difficult to form nanocracks longer than a few nanometers. The reason for this is that as r_0 increases, the stress caused by the load applied to the plane of the nanocrack decreases. This decrease in applied load-induced stresses has a large effect on the growth of nanocracks, correspondingly, as r_0 increases, the Burgers vector also increases.

Thus, the following is shown within the framework of the model [38]. First, the conditions for the origin and growth of nanocracks in nanocrystalline materials become easier with an increase in the radius of curvature (Fig. 12). This means that blunt cracks do not effectively affect the brittleness of nanocrystalline materials. As a rule, it is the micromechanism associated with the high degree of plasticity and viscous dissipation in traditional polycrystalline metals. On the other hand, the origin and growth of nanocracks in nanocrystalline materials is more evident with decreasing grain size (Fig. 13). In other words, decreasing the grain size reduces the plasticity of nanocrystalline materials.

Figure 14 shows the dependences of $q(l)$ on different angle values $\beta=\pi/4,\pi/2,\pi$ corresponding to $r_0=1.0\text{nm}$, $r_0=1.2\text{nm}$, $r_0=1.4\text{nm}$, $r_0=1.6\text{nm}$ values for hybrid FML composites with 0.2% clay addition. As it can be seen from the graph, as the angle values increase, the crack growth increases accordingly.

Experimental data, computer and theoretical modeling results on nanocrack formation in metal matrix hybrid nanocomposite materials under the influence of high-speed and quasi-static deformation regimes were compared with studies in the literature. Typical elementary cracks in nanocomposite materials are formed in dislocation stress fields as a result of intergranular sliding at grain boundaries. Elliptical cracks (Fig. 11) are typical carriers of the fragmentation process [39-40]. In nanocomposite materials, cracks often form and grow along curved grain boundaries [41]. Nanocomposite materials exhibit special behavior when subjected to high-speed deformation [42-43].

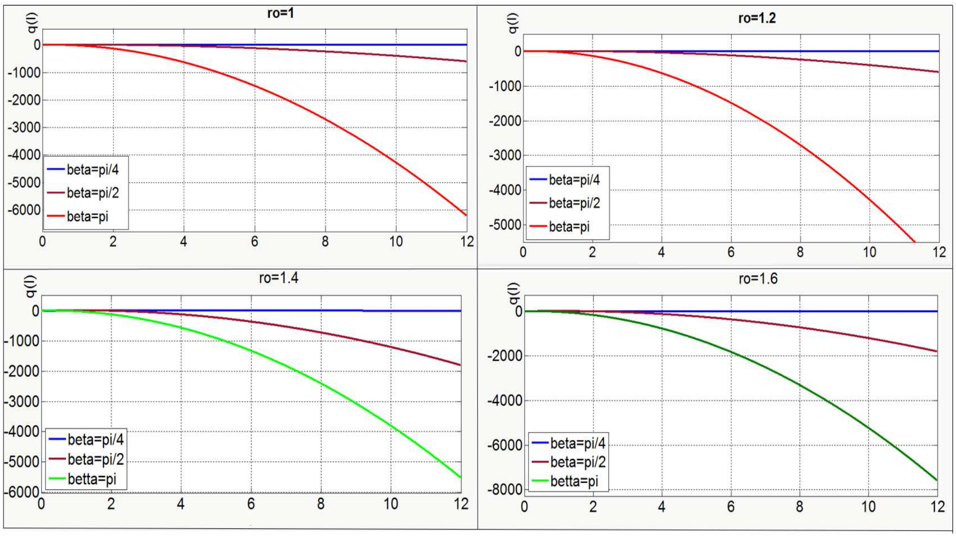

Fig. 12. Dependences of the charge q on the crack length l at different angular values of β corresponding to different values of r_0 for the hybrid nanocomposite with 0.2% clay addition. The horizontal line the value of the load q_c = 272.307.

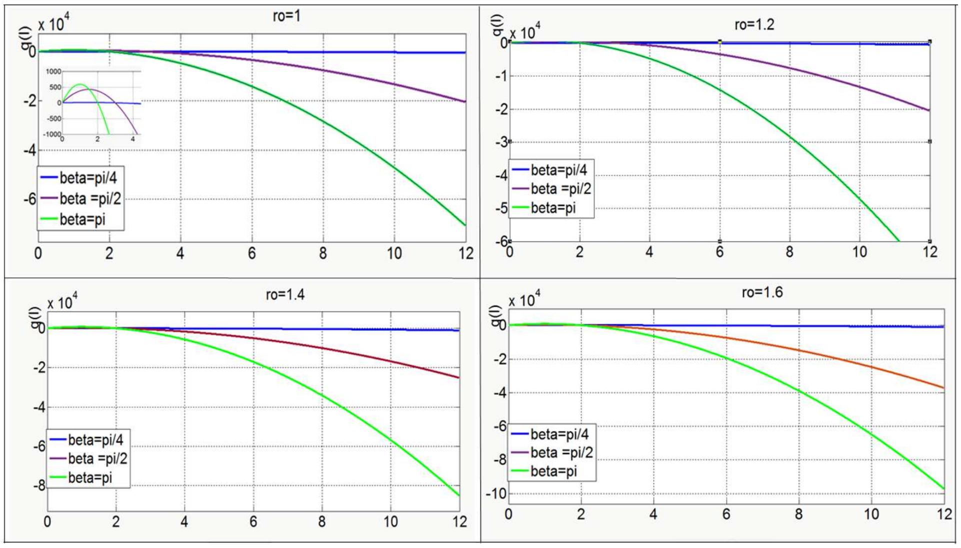

Fig. 13. Dependences of the charge q on the crack length l at different angular values of β corresponding to different values of r_0 for the hybrid nanocomposite with 0.2% SiO_2 addition. The horizontal line the value of the load q_c = 377.880.

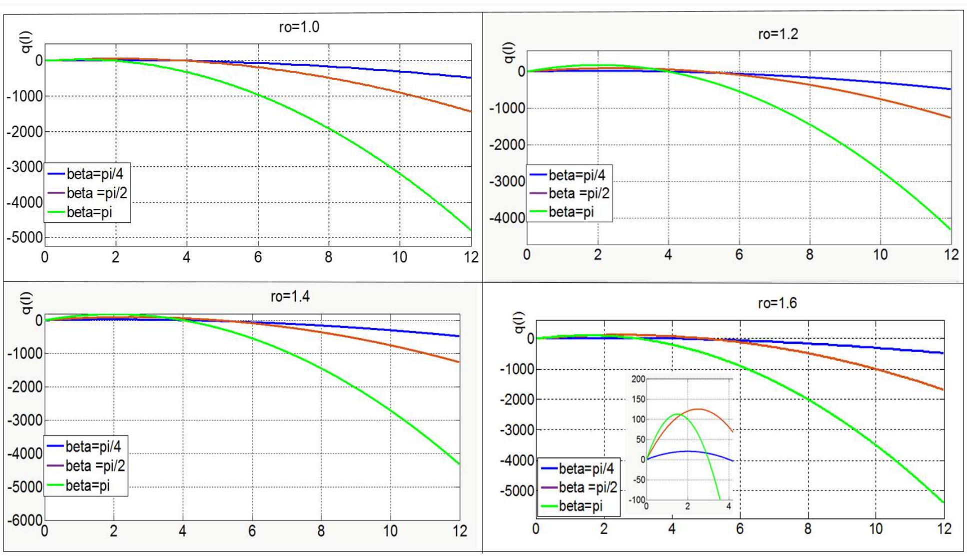

Fig. 14. Dependences of the charge q on the crack length l at different angular values of β corresponding to different values of r_0 for the hybrid nanocomposite with 0.2% GNP addition. The horizontal line the value of the load q_c = 167.432.

4. Conclusions

Theoretical and experimental tensile tests of hybrid FML composites were carried out according to ASTM D3039M-17 and the effects of nanoparticles used in composites on nanocracks formed under the influence of tensile test and quasi-static deformation regimes were examined and the following conclusions were reached:

1. In the tensile test of hybrid FML composites with the help of ANSYS program, the maximum deformation value was 0.62527 mm and it occurs on “7075-T6 Al”. The maximum equivalent tensile value is 958.29 MPa and it occurs on “Carbon fiber fabric”. At the same time, the maximum value of the equivalent elastic stress is 1.3481 mm/mm and it occurs on the “Carbon fiber fabric”.
2. As a result of the tensile tests, the tensile strength of 0.2% clay reinforced hybrid FMLs was observed to be 914.2 MPa, an increase of approximately 0.3% compared to hybrid FMLs produced with pure epoxy resin. It was observed that the 0.2% GNP reinforcement composite provided a 0.3% increase in tensile strength saddles and the strength value was 918.5 MPa. It was observed that 0.2% SiO_2 nanoparticle reinforcement to pure epoxy resin in hybrid FMLs increased the tensile strength of the composite sample by 2.1% to 931.7 MPa. Improved tensile strength properties were observed in hybrid FML composites due to the incorporation of nanoparticles into the pure epoxy resin, improved adhesion properties and crack quenching mechanisms between matrix and fibers.
3. It was observed that the difference between the tensile test results obtained in the 3D simulation experiment of hybrid FML composites and the experimental results was less than 5%, which is an acceptable value. Modeling of tensile of this sample allowed to study in more detail the mechanical properties of this hybrid FML composite material.
4. The formation and growth of nanocracks in nanocomposite materials is explained by the decrease in grain size. In other words, the decrease in grain size reduces the plasticity of the nanocomposite material. The decrease in grain size in nanocomposite metals corresponds to the experimentally observed viscous-brittle transition. The obtained results confirm the experimental results on low viscosity and plasticity of most nanocomposite materials.

Author Contributions

N. Gurbanov conducted the production of samples in laboratory conditions and tensile tests according to ASTM D3039M-17 standard and analyzed the results; M. Babanli analyzed the results from the simulation and experiment; Y. Turen corrected the manuscript; R. Mehtiyev investigated experimental data, computer and theoretical models of nanocrack formation processes in nanocomposite materials under the influence of high-speed and quasi-static deformation regimes; M.Y. Askin provided technical interpretation for conducting the experiments; M. Ismayilov developed, a 3D numerical model of hybrid FML, inside ANSYS Workbench Explicit Dynamics modulus and used it to predict their strengths according to the ASTM D3039M-17 standard; all authors contributed in writing and approved the final version of the manuscript.

Acknowledgments

Not Applicable.

Conflict of Interest

The authors declared no potential conflicts of interest concerning the research, authorship, and publication of this article.

Funding

The authors received no financial support for the research, authorship, and publication of this article.

Data Availability Statements

The datasets generated and/or analyzed during the current study are available from the corresponding author on reasonable request.

Nomenclature

σ_0	Tensile load	A	The work of the bias voltage caused by an external charge to form a dislocation dipole
b	Burgers vector	r_c	Radius of the dislocation core
ρ	Radius of curvature of the crack	$\sigma_{r\theta}^{dip}$	Stress tensor component
a and p	Semi-axes of the ellipse	$\sigma_{r\theta}^{e}$	Stress tensor component
α	The angle between the grain boundary and the crack plane where slip occurs	σ_0	Load near the tip of an elliptical crack
ΔW	The minimum energy associated with the formation of a dipole	b_c	The equilibrium (max) value of the modulus of the Burgers vector b
W_S	Internal elastic energy of the dislocation dipole	ρ_c	Crack tip ρ exceeds some critical value
W_C	The energy of the dislocation core with the Burgers vector b	γ	Specific energy of the free surface
σ_{0c}	External stress σ_0 maximum value	l	Length of nanocrack
$\phi_e(z), \psi_e(z)$	Complex potentials	F	Configuration force
$\sigma\,\alpha\,\theta\,r\,r$	Stress field created by a dislocation located at point B	γ	The specific energy of the grain boundary
$\sigma\,\alpha\,\theta\,\theta$	Stress field created by a dislocation, the core of which is “smeared” inside an elliptical crack	τ	The vector directed from the dislocation line along the nanocrack
$\sigma_{yy}^d, \sigma_{nn}^d$	Stress tensor component	n	The normal directed vector to the nanocrack
$\overline{\sigma}_{nn}, \overline{\sigma}_{\tau n}$	Stress tensor component		
$\sigma_{nn}, \sigma_{\tau n}$	Weighted average stress values		

References

[1] Gurbanov, N.A., Babanli, M.B., Investigation of Effects of Graphene Nanoplatelets Addition on Mechanical Properties of 7075-T6 Aluminium Matrix Hybrid Fibre Metal Laminates, *Metallophysics and Advanced Technologies*, 43(12), 2021, 1589-1599.
[2] Asundi, A., Choi, A.Y.N., Fiber metal laminates: An advanced material for future aircraft, *Journal of Materials Processing Technology*, 63(1), 1997, 384-394.
[3] Baltaci, A., Sarikanat, M., Yildiz, H., Static stability of laminated composite circular plates with holes using shear deformation theory, *Finite Elements in Analysis and Design*, 43(11), 2007, 839-846.
[4] Dong, C., Multi-objective Optimal Design of Carbon and Glass Reinforced Hybrid Composites under Flexural Loading, *Journal of Applied and Computational Mechanics*, 8(4), 2022, 1324-1331.
[5] Botelho, E.C., Silva, R.A., Pardini, L.C., Rezende, M.C., A review on the development and properties of continuous fiber/epoxy/aluminum hybrid composites for aircraft structures, *Materials Research*, 9(3), 2006, 247-256.
[6] Gurbanov, N., Askin, M.Y., Babanli, M., Turen, Y., An investigation of mechanical properties of different nanoparticle reinforced 7075-T6 Al matrix hybrid fiber metal laminated composites, *Functional Materials*, 29(1), 2022, 172-181.
[7] Huang, S.H., Penk, L., Abhiram, M., Liang, H., Additive Manufacturing and Its Societal Impact:A Literature Review, *The International Journal of Advanced Manufacturing Technology*, 67(5), 2013, 1-25.
[8] Brown, M.A., Seugling, M.R., Using Plate Finite Elements for Modeling Fillets in Global Response Analysis, *Finite Elements in Analysis and Design*, 40, 2004, 1963-1975.
[9] Randjbaran, E., Majid, D.L., Zahari, R., Sultan, M.T., Mazlan N., Effects of volume of carbon nanotubes on the angled ballistic impact for carbon kevlar hybrid fabrics, *Facta Universitatis, Series: Mechanical Engineering*, 18(2), 2020, 229-244.
[10] Elizalde, H., Cárdenas, D., Delgado-Gutierrez, A., Probst O., In-plane shear-axial strain coupling formulation for shear- deformable composite thin-walled beams, *Journal of Applied and Computational Mechanics*, 7(2), 2021, 450-469.
[11] Barbero, E.J., Shahbazi, M., Determination of material properties for ANSYS progressive damage analysis of laminated composites, *Materials Today: Proceedings*, 176, 2017, 768-779.
[12] Abisset, E., Daghia, F., Ladeveze, P., On the validation of a damage mesomodel for laminated composites by means of open-hole tensile tests on quasi-isotropic laminates, *Composites Part A*, 42(10), 2011, 1515-1524.
[13] Ali, K.S.A., Manuel, J.D., Balamurugan, M., Murugan, M.S., Analysis of composite leaf spring using ANSYS software, *Materials Today: Proceedings*, 37(2), 2021, 2346-2351.
[14] Asadollahi, Y.E., Gardan, J., Lafon, P., Integrated design in additive manufacturing based on design for manufacturing. *Int'l Journal of Mechanical, Aerospace, Industrial, Mechatronic and Manufacturing Engineering*, 10(6), 2016, 1104-1111.
[15] Azizpooryan, M., Noormohammadi, N., Boroomand, B., Equilibrated Basis Functions for Static Analysis of In-plane Heterogeneous Laminated Composite Plates in Boundary and Meshfree Approaches, *Iranian Journal of Science and Technology - Transactions of Mechanical Engineering*, 46, 2022, 957–984.
[16] Bhagat, V.S., George, N., Arunkumar, M.P. et al., Numerical Analysis on Vibro-Acoustic Behavior of Honeycomb Core Sandwich Structure with FG-CNT-Reinforced Polymer Composite Facings, *Iranian Journal of Science and Technology - Transactions of Mechanical Engineering*, 46, 2022, 943–956.
[17] Rastgaar, A.M., Mahinfalah, M., Nakhaie, J.G., Linear static analysis and finite element modeling for laminated composite plates using third order shear deformation theory, *Composite Structures*, 62(1), 2003, 27-39.
[18] Onyibo, E.C., Safaei, B., Application of finite element analysis to honeycomb sandwich structures: a review, *Reports in Mechanical Engineering,* 3(1), 2022, 192-209.
[19] Askin, M.Y., Turen, Y., The effect of GNP addition on mechanical and residual stress properties of 2024-T3 aluminum and carbon fiber reinforced FML, *Materials Research Express*, 6, 2019, 126546
[20] Babanli, M.B., Gurbanov, N.A., Mehtiyev, R.K., Formation and Growth of Cracks in 7075-T6 Aluminium Matrix Hybrid FML Nanocomposite Materials, *Progress in Physics of Meterials*, 23(3), 2022, 489-509.
[21] Conrad, H., Narayan, J., Mechanism for grain size softening in nanocrystalline Zn, *Applied Physics Letters*, 81(12), 2002, 2241.
[22] Demkowicz, M.J., Argon, A.S., Farkas, D., Frary, M., Simulation of plasticity in nanocrystalline silicon, *Philosophical Magazine*, 87(28), 2007, 4253.
[23] Gutkin, M.Yu., Ovid'ko, I.A., Effect of triple junctions of nanotubes on strengthening and fracture toughness of ceramic nanocomposites, *Physics of the Solid State*, 52, 2010, 1397-1403.
[24] Meyers, M.A., Mishra, A., Benson, D.J., Mechanical properties of nanocrystalline materials, *Progress in Materials Science*, 51, 2006, 427–556.
[25] Padilla, H.A., Boyce, B.L., A Review of Fatigue Behavior in Nanocrystalline Metals, *Experimental Mechanics*, 50, 2010, 5-23.
[26] Faizan, M., Gangwar, S., Tensile behaviour of carbon fiber reinforced polymer composite using ANSYS 21, *Materials Today: Proceedings*, 46(15), 2021, 6519-6526.
[27] Binu, P.P., Georgeb, E., Vinodkumara, M.N., Effect of nanoclay, Cloisite15A on the Mechanical Properties and Thermal behavior of Glass Fiber Reinforced Polyester, *Procedia Technology*, 25, 2016, 846-853.
[28] Sydlik, S.A., Lee, J.H., Walish, J.J., Thomas, E.L., Swager, T.M., Epoxy functionalized multi-walled carbon nanotubes for improved adhesives, *Carbon*, 59, 2013, 109-120.
[29] Afrouzian, A., Aleni, H., Hossein, G., Ahmadi, H., Effect of nano-particles on the tensile, flexural and perforation properties of the glass/epoxy composites, *Journal of Reinforced Plastics and Composites*, 36(12), 2017, 900-916.
[30] Ovid'ko, I.A., Sheinerman, A.G., Cracks at disclinated grain boundaries in graphene, *Journal of Physics D: Applied Physics*, 46(34), 2013, 345305.
[31] Repetsky, S.P., Len, E.G., Lizunov, V.V., *Metallofiz. Noveishie Tekhnol.*, 28(8), 2006, 989.
[32] Mura, T., *Micromechanics of Defects in Solids*, Dordrecht: Springer–Kluwer Academic, 1987.
[33] Zhuang, Z., Liu, Z., Cui Y., *Dislocation Mechanism-Based Crystal Plasticity: Theory and Computation at the Micron and Submicron Scale*, Academic Press, 2019.
[34] Fischer, L.L., Beltz, G.E., The effect of crack blunting on the competition between dislocation nucleation and cleavage, *Journal of the Mechanics and Physics of Solids*, 49(3), 2001, 635-654.
[35] Beltz, G.E., Lipkin, D.M., Fischer, L.L., Role of Crack Blunting in Ductile Versus Brittle Response of Crystalline Materials, *Physical Review Letters*, 82(22), 1999, 4468.
[36] Ovid'ko, I.A., Sheinerman, A.G., Ductile vs. brittle behavior of pre-cracked nanocrystalline and ultrafine-grained materials, *Acta Materialia*, 58(16), 2010, 5286-5294.
[37] Barenblatt, G.I., The Mathematical Theory of Equilibrium Cracks in Brittle Fracture, *Advances in Applied Mechanics*, 7, 1962, 55-129.
[38] Khan, A.S., Suh, Y.S., Kazmi, R., Quasi-static and dynamic loading responses and constitutive modeling of titanium alloys, *International Journal of Plasticity,* 20(12), 2004, 2233-2248.
[39] Khana, A.S., Suha, Y.S., Chena, X., Takacs, L., Zhanga, H., Nanocrystalline aluminum and iron: Mechanical behavior at quasi-static and high strain rates, and constitutive modeling, *International Journal of Plasticity*, 22(2), 2006, 195-209.
[40] Hulbert, D.M., Jiang, D., Kuntz, J.D., Kodera, Y., Mukherjee, A.K., A low-temperature high-strain-rate formable nanocrystalline superplastic ceramic, *Scripta Materialia*, 56(12), 2007, 1103-1106.
[41] Guo, J., He, L., Liu, Y., Li, L., Anti-plane analysis of a reinforced nano-elliptical cavity or nano-crack in a magnetoelectroelastic matrix with surface effect, *Theoretical and Applied Fracture Mechanics*, 107, 2020, 102553.
[42] Liu, D., Cherns, D., Nano-cracks in a synthetic graphite composite for nuclear applications, *Philosophical Magazine*, 98(14), 2018, 1272-1283.
[43] Daia, K., Shaw, L., Analysis of fatigue resistance improvements via surface severe plastic deformation, *International Journal of Fatigue*, 30(8), 2008, 1398-1408.

ORCID iD

Mustafa Babanli https://orcid.org/0000-0003-1939-6511
Nurlan Gurbanov https://orcid.org/0000-0003-3152-1442

Yunus Turen https://orcid.org/0000-0001-8755-1865
Rafail Mehtiyev https://orcid.org/0000-0002-8061-9641
Mustafa Yunus Askin https://orcid.org/0000-0002-5753-2804
Mahmud Ismayilov https://orcid.org/0000-0002-7835-7590

How to cite this article: Babanli M., et al. Theory and Experiment in Predicting the Strength of Hybrid Fiber Metal Laminates, *J. Appl. Comput. Mech.*, 9(4), 2023, 987–999. https://doi.org/10.22055/jacm.2023.42798.3978